# One-sided transform basins and "inverted curtains": Implications for releasing bends along strike-slip faults

Eunseo Choi,[1] Leonardo Seeber,[1] Michael S. Steckler,[1] and Roger Buck[1]

Received 11 May 2011; revised 29 August 2011; accepted 2 September 2011; published 9 November 2011.

[1] Some basins associated with bends along strike-slip faults grow only on one side of the fault. We ascribe this asymmetry to a characteristic 3D geometry. The strike-slip fault is planar and vertical, except at the "inverted curtain" where the fault has a sinusoidal bend that decreases linearly downward and vanishes below a prescribed depth. We model numerically the deformation around inverted curtains with different dips. We consider a crustal block traversed by a fault with lower cohesion than the surrounding rock and subject it to strike-slip motion, first with purely elastic models and then with Mohr-Coulomb elasto-plastic ones. We found that when a curtain is vertical, both sides of the bend subside forming a symmetrical basin. In contrast, basins are formed only on the hanging wall side of a releasing bend of a non-vertical curtain, in agreement with field examples. For the same curtain geometries, the basins are broader and shallower in an elastic crust than in an elastic-plastic one. While releasing bends are stable over a range of dips, restraining bends are "shunted" by new straight faults except in shallow-dipping curtains. These model results show that bends on transcurrent faults with inverted curtain geometries lead to asymmetric ridges and basins. Conversely, such a characteristically asymmetric basin (ridge) is symptomatic of a transform bend with oblique slip that attenuates with depth and is rooted below the subsided (uplifted) area. One implication is that master transcurrent faults may remain primarily or solely responsible for earthquake hazard along segments with anomalous vertical deformation.

**Citation:** Choi, E., L. Seeber, M. S. Steckler, and R. Buck (2011), One-sided transform basins and "inverted curtains": Implications for releasing bends along strike-slip faults, *Tectonics*, *30*, TC6006, doi:10.1029/2011TC002943.

## 1. Introduction

[2] Relative motion along continental transform faults is dominantly horizontal, but locally includes large vertical components. Transform basins and ridges are ubiquitous: 195 active ones have been globally cataloged by *Mann* [2007]. The terms "pull-apart basins" and "push-up ridges" have structural connotations and refer to the causative role of the transform fault. Deviations from straight, continuous geometries of this master fault, typically "extensional" and "compressional" jogs, bends, or offsets, locally perturb kinematics. Resistance to volume changes causes subsidence (thinning) or uplift (thickening), which lead to pull-apart basins or push-up ridges, respectively. Hydrocarbon reservoir potential [e.g., *Crowell*, 2003] and segmentation of damaging strike-slip earthquake ruptures (e.g., 1999 earthquake pair in Turkey [*Pantosti et al.*, 2008]) have contributed to the long-term interest in these structures.

[3] Surface structure and morphology show that transform geometries leading to horizontal shortening or extension consistently produce uplift and subsidence, respectively. Beyond this obvious qualitative correlation, however, specifics on 3D fault geometries and their evolution in pull-apart basins and push-up ridges are still unclear and models have tended to be conceptual rather than driven by data. For instance, strike-slip faults are often nearly vertical and a bend or a "jog" on a vertical fault with pure strike-slip offset develops a stress anomaly symmetrical to the jog. Not surprisingly, pull-apart basins were therefore generally expected to be symmetrical [e.g., *Dibblee*, 1977; *Segall and Pollard*, 1980].

[4] Improved data, however, often show systematic asymmetries of pull-apart basins, for which simple 2D models are inadequate. However, they have not yet spawned widely accepted alternatives. Lack of consensus characterizes even some well documented cases, such as the transtensive regime of the Marmara Sea [e.g., *Armijo et al.*, 1996, 1999; *Le Pichon et al.*, 2001; *Okay and Okay*, 2002; *Okay et al.*, 2000; *Seeber et al.*, 2004, 2006] and the transpressive regime along the Enriquillo-Plaintain Garden transform fault that may or may not have ruptured in the catastrophic 2010 earthquake in Haiti [*Calais et al.*, 2010; *Prentice et al.*, 2010; *Hornbach et al.*, 2010; *Hayes et al.*, 2010, L. Seeber et al., The January 2010 Haiti mainshock-aftershock sequence: Positive feedback between faults in slip-partitioned transpression, submitted to *Geology*, 2011], where conflicting

[1]Lamont-Doherty Earth Observatory, Palisades, New York, USA.


0278-7407/11/2011TC002943

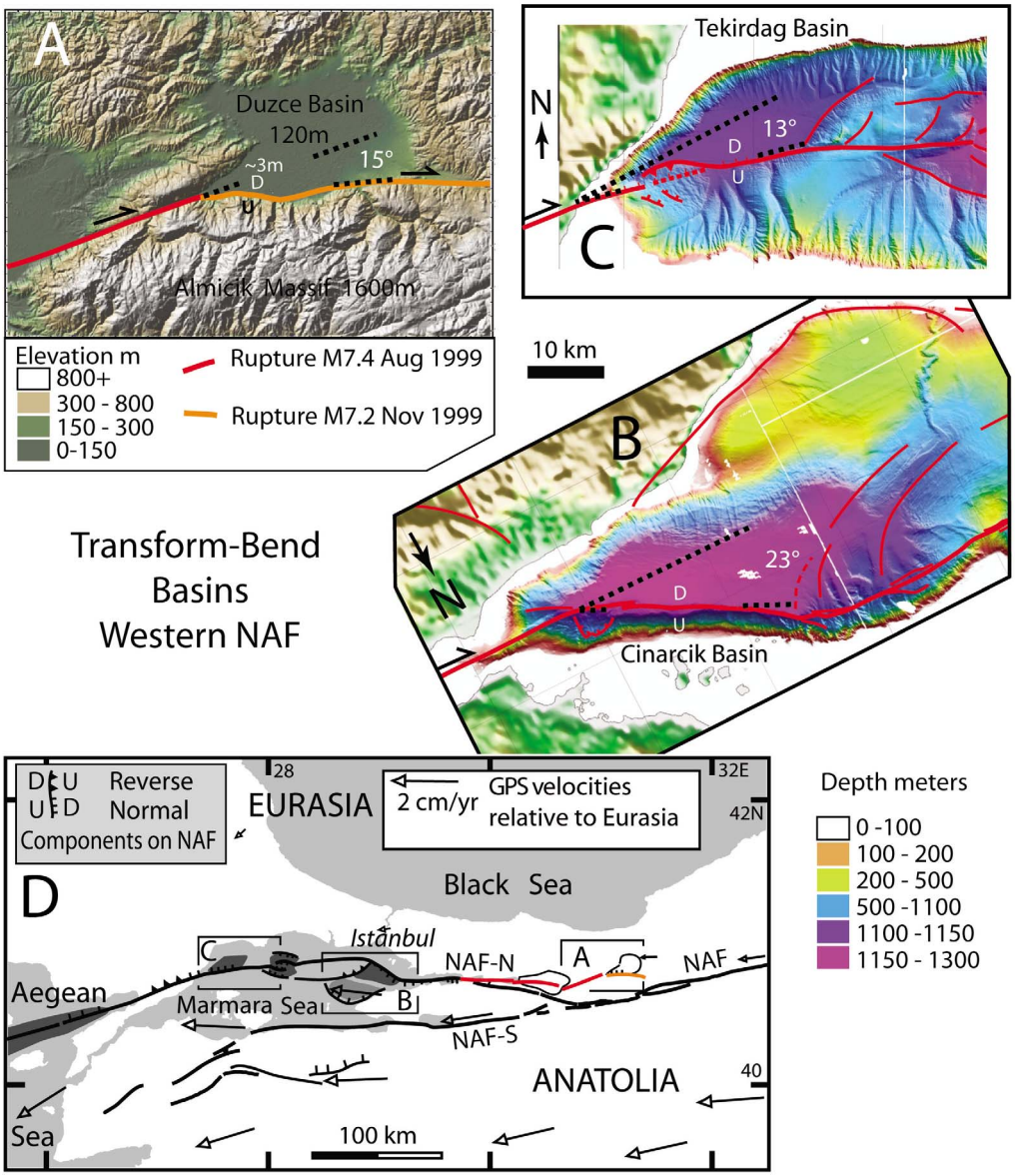


**Figure 1.** (a–d) Examples of transform-bend basins (Figures 1a–1c at same scale; locations are in Figure 1d) along the northern branch of the North Anatolian Fault (NAF-N) in western Turkey. At all these bends, this dextral continental transform is non-vertical and slips obliquely with a normal component (U = up; D = down). The basins are triangular with the apex near the bend, where they subside fastest. They form by tilting toward the bend and toward the fault on the hanging wall side and are characteristically asymmetric.

geometries are still being debated. A wide range of strike-slip fault geometries can translate horizontal into vertical strain. The three main models are: 1) fault bends with no strain partitioning, e.g., Ridge Basin [*Crowell*, 2003]; 2) fault jogs with strain partitioning, e.g., Central Marmara Basin [*Armijo et al.*, 1996, 1999]; 3) vertical-axis block rotation, e.g., Imperial Valley [*Nicholson and Seeber*, 1989]. Distinguishing among these and other structural models requires matching of detailed predictions of the expected deformation patterns with structural data.

[5] Recent data from the North Anatolian transform fault in the Marmara Sea have pointed to a class of transform-bend related basins with some surprising characteristics (Figure 1). They include, biaxial asymmetry that has been interpreted to stem from oblique slip on a non-vertical transform fault at the bend (i.e., no strain partitioning), and unilateral growth that implies off-fault deformation confined to one side of the transform fault. These basins and the causative fault bends advance at the speed of transform fault to remain stationary relative to the opposite side of the fault [*Seeber et al.*, 2010]. Similar characteristics have been described on fossil [*Crowell*, 2003] and active basins [*Wakabayashi*, 2007] along the San Andreas transform fault. Near the causative fault bend, subsidence can be extremely rapid, approach-

ing the horizontal velocity of the transform fault, but it is time transgressive, propagating toward the bend. These features suggest specific 3D fault geometries and basin growth that can be tested. The purpose of this paper is to construct realistic 4D mechanical models that can produce finite strain fields associated with specific anomalies in transform fault geometries. By reproducing some of the natural observations, we hope to constrain both transform fault geometry and fault mechanics.

[6] Realistic numerical modeling of 3D basin formation due to non-planar fault geometry is challenging. Including discontinuous structures with non-trivial geometries in a mechanical continuum requires special treatment in both meshing the space and in setting the constitutive model. Also, 3D models incur high, sometimes prohibitive, numerical cost. To overcome one or more of these difficulties, some 3D models focus on acquiring instantaneous or steady state solutions for a pre-defined fault geometry [e.g., *Li et al.*, 2009; *Hergert and Heidbach*, 2010; *Katzman et al.*, 1995]. Another successful approach to tectonics related to non-planar faults is analog modeling [e.g., *Wu et al.*, 2009]. This experimental technique has allowed monitoring the growth of complex realistic structures through large deformation and has yielded results generally consistent with numerical models. However, discrepancies have also been reported between numerical and analog models and even between analog models with similar settings [*Buiter et al.*, 2008]. Numerical models can uniquely crosscheck among competing results and hypotheses and can also handle 3D settings with precise control on subtle differences in geometry and physics. This process has just started for fault-controlled basins, given the recent advances in the ability to produce such basins numerically through finite time-dependent deformation on non-trivial 3D fault geometries [e.g., *Ben-Avraham et al.*, 2010].

[7] Transform basins have been associated with "releasing" bends, where horizontal fault slip increases horizontal area and must thus also cause subsidence in order to conserve volume (Figure 1) [e.g., *Mann*, 2007]. The Cinarcik and Tekirdag basins in the Marmara Sea and other basins along the North Anatolian Fault in western Turkey have been intensely investigated after the two destructive earthquakes in 1999 (Figure 1) [e.g., *Okay et al.*, 1999, 2004; *Le Pichon et al.*, 2001; *Bécel et al.*, 2010; *Carton et al.*, 2009; *Seeber et al.*, 2004, 2006; *Cormier et al.*, 2006]. The diverse data available, including bathymetry and seismic profiles, show that most of these basins have developed asymmetrically and unidirectionally on the concave and releasing side of bends along the North Anatolian Fault (NAF) (Figure 1). Based on these observations and other examples along the San Andreas Fault system, *Seeber et al.* [2010] suggested that these one-sided asymmetrical transform basins might stem from a characteristic fault geometry.

[8] *Seeber et al.* [2004] proposed models to account for these asymmetric basins in which causative bends on the strike-slip faults attenuate and vanish with depth. Structural and/or lithologic perturbations in the upper crust can easily account for such shallow warping of the faults. These warps can exist from the onset as pre-existing faults inherited from older regimes. They can also form syn-tectonically as a result of kinematic or mechanical anomalies. A strike-slip fault may warp because of interaction with other "incompatible" active faults in a strain-partitioned system (Seeber et al., submitted manuscript, 2011), or in response to downslope collapse [*Eusden et al.*, 2000], or as it locally deviates through weaker material.

[9] There are extreme views about the strength of faults. Faults are known to have friction coefficients between 0.6 and 0.8 in some conditions [e.g., *Byerlee*, 1978]. Stress differences measured in boreholes around the world indicate that friction coefficients are on this level [e.g., *McGarr and Gay*, 1978; *Brace and Kohlstedt*, 1980; *Townend and Zoback*, 2000]. However, there is evidence that some faults have much lower coefficients of friction. The orientation of stresses close to the San Andreas Fault [e.g., *Mount and Suppe*, 1987; *Zoback and Healy*, 1992] and the lack of a localized heat flow anomaly over the San Andreas [*Lachenbruch and Sass*, 1992] argue for weak faults. Large-offset on low-angle normal faults, or detachments in metamorphic core complexes [e.g., *Coney*, 1980], would also imply that they are weak [e.g., *Wernicke*, 1981; *Davis and Lister*, 1988]. We have poor constraints on how fault strength changes with continued slip. Our results show that fault mechanics is critical in the model behavior and is the area that needs most improvement, although recent papers suggest that shear fabric contributes to weakening of faults [*Collettini et al.*, 2009; *Niemeijer et al.*, 2010]. In spite of these uncertainties as to fault strengths, it is often assumed in numerical models that either cohesion or friction coefficient is reduced with offset (i.e., strain-weakened) by an arbitrarily sufficient amount. Benchmarking numerical models against the detailed record of evolution of some well-studied transform basins can provide constraints on fault strength.

[10] In this study, we use a 3D numerical code to model basin growth due to bends along a strike-slip fault. The hypothesis to be tested is that a basin can form asymmetrically solely due to the sub-surface geometry of the fault. We explore the vertical component of deformation at the surface as a result of 3D fault bends that decrease downward and vanish at depth.

## 2. Model Setup

### 2.1. Inverted Curtain Structure and Its Variants

[11] A block of continental crust is cut longitudinally by a vertical fault, which is warped locally to form a subtle bend along the surface trace of the fault (Figure 2). We consider only the case of a bend that vanishes at a horizontal line below which the fault becomes vertical and planar. We term this structure an "inverted curtain," or simply, "curtain." The warp is an inverted curtain that linearly attenuates with depth and vanishes at a prescribed depth. We consider the case of a strike-slip fault that is perfectly oriented to absorb the prescribed transform motion with horizontal slip except for this geometric perturbation ("asperity") in the shallow part of the fault. Here we consider inverted curtain geometries whose surface traces fit into two well-known classes of structures: (1) A single releasing bend; and (2) paired releasing and restraining bends.

[12] The geometry of an inverted curtain associated with a paired bends is defined by length ($L$), amplitude ($W$), and depth ($D$) (Figure 2a). The bend geometry is defined as $z' = 0.5w(y)\cos(2\pi x'/L)$, where $z'$ and $x'$ are domain-centered coordinates for the bend along the $z$ and $x$ axis, respectively, the $y$ coordinate is positive upward and 0 at the initial top

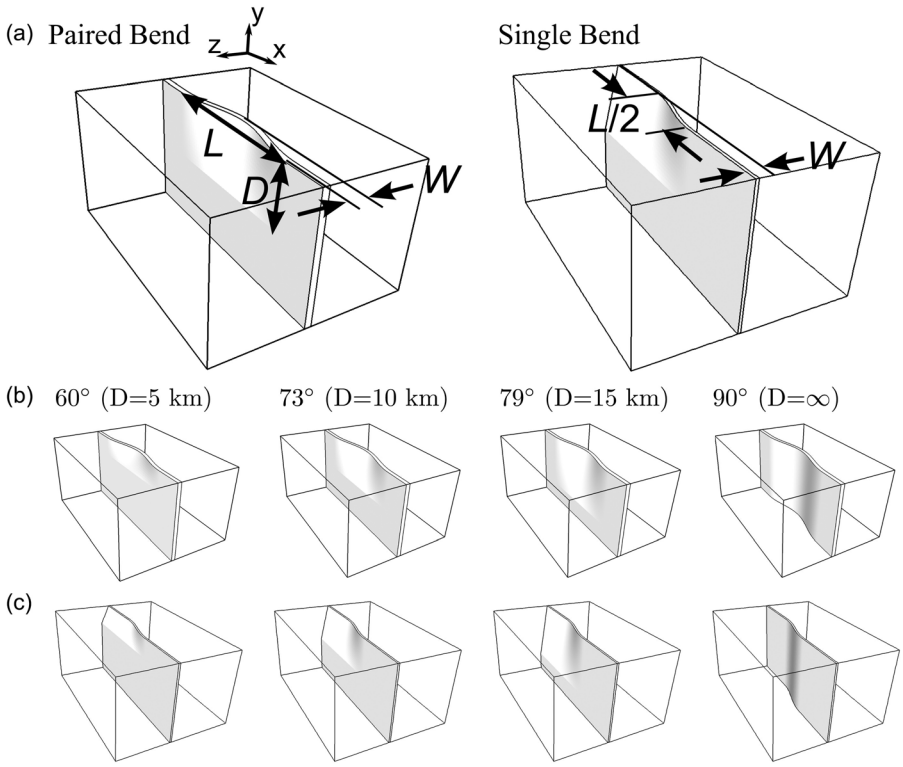


**Figure 2.** Geometry of inverted curtains on a strike-slip fault. (a) Three parameters that determine the geometry of a paired or a single bend. (b) Four paired releasing-restraining bends with different dip angles and (c) the corresponding single releasing bends. $W$ and $L$ are fixed at 3 km and 27 km in all experiments. $D$ is varied and determines the dip angle of a curtain.

surface, and the bend extends from $-L/2 \le x' \le L/2$. The half amplitude is placed on the median plane along the $y$ axis and the maximum bulge is centered along the $x$ axis. The amplitude, $w(y)$, diminishes linearly with depth ($y$) and becomes zero at the depth $y = -D$: $w(y) = W(1 - |y|/D)$. Grid spacing is adjusted such that fault zone boundaries coincide with grid surfaces. The dip angle of a curtain is defined as $\tan(D/W)$. $L$ = 27 km and $W$ = 3 km for all the models. We choose four values of $D$: 5, 10, 15 km and infinity. The corresponding dip angles are 60°, 73°, 79° and 90°, respectively (Figure 2b).

[13] To simulate a larger distance between the releasing and restraining bends, we also set up models with a single releasing bend. The bend geometry is again defined by three parameters, $L$, $W$, and $D$. The geometry is given by $z' = 0.5w(y)\sin(2\pi x'/L)$ where $x'$ has the range, $-L/4 \le x' \le L/4$. $L$, $W$, and $D$ take the same values as for the paired bends. The resultant curtain structures are shown in Figure 2c. Both paired-bend and single-bend models have geologic counterparts in the Marmara Sea area and elsewhere. The single releasing bend is simpler and thus more useful for isolating processes. We will discuss it first.

### 2.2. Elastic Crust Model With Kinematic Fault Slip

[14] To understand the first-order behavior of this geometric model, we consider the deformation of a linear elastic crust driven by kinematic loadings on the boundaries. To isolate the crustal response to transtensive and transpressive loadings on the bends, we apply constant slip rates on the fault as well. With the combination of these loading conditions, crustal blocks would simply translate as rigid blocks if the fault was perfectly straight. The complicated fault geometry requires the use of numerical methods for solving the problem and we use PyLith, a finite element code for simulating crustal deformation due to kinematic boundary loading as well as distributed slip on faults [*Aagaard et al.*, 2007, 2008; *Williams*, 2006; *Williams et al.*, 2005].

[15] The model domain, covering an area of 80 × 32 km and 20 km-thick, is discretized into 40 × 16 × 10 hexahedral linear elements for most of the calculations. A zero-thickness fault with a curtain geometry is assumed to slip only in the local strike-slip direction but not in the fault-normal or dip directions. However, the fault can move as the surrounding area deforms. We impose right-lateral motion with the rate of 2 cm/yr on two fault-parallel domain boundaries ($xy$ planes) with the normal component of velocity ($v_z$) set to be zero (Figure 3a). The $z$ component of velocity is set to be zero on the two fault-normal domain boundaries ($yz$ planes) so that there is no rotation around the vertical axis at the end of the model fault plane. The slip rates imposed on the fault are set to be equal to the applied far-field strike-slip motion but projected onto the fault surface where the fault's strike is not parallel to the applied strike-slip motion. Gravitational load is not considered because we are interested only in stress changes. The bottom and top boundaries are free surfaces. All the models were run until the total applied

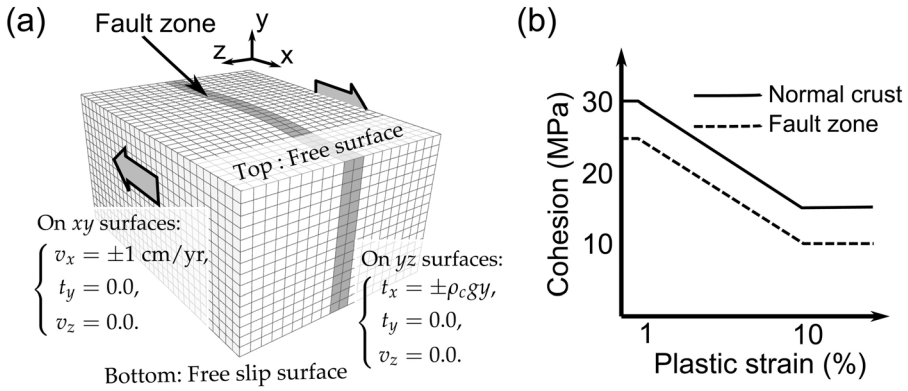


**Figure 3.** (a) Geometry of the elasto-plastic domain and boundary conditions. The fault zone is marked by a group of elements with dark gray shading. Big arrows filled with light gray show the sense of applied strike-slip motion. $t_x$ and $t_y$ denote $x$ and $y$ components of traction, respectively. Note that the grid spacing shown is twice the actual spacing. (b) Strain weakening applied in the elastic-plastic cases in this study.

right-lateral motion reached 3 km. Both Lamé's constants are 30 GPa.

### 2.3. Elasto-Plastic Crust Model

[16] The accumulated structure in transform basin and ridges typically involve large vertical deformations, which are clearly non-elastic and models that account for yielding and permanent deformation are more realistic than elastic models. Another justification for an elasto-plastic model is that the "effective" material properties in these models are sufficient to describe the behavior of discontinuities like faults as well as the bulk material that includes them. The finite yield strength of the lithosphere is known to reduce the wavelength of lithospheric bending [e.g., *McAdoo et al.*, 1978] and may similarly affect the dimensions of transform basins. Also, assuming that yield strength is reduced with increasing strain allows development of secondary faults in the model. Strain weakening (or softening) plasticity is a constitutive model for materials whose strength decreases with strain (i.e., negative stiffness) after yielding. Such behavior has been shown to unconditionally cause strain-localization [*Rudnicki and Rice*, 1975]. Faults and cracks are often modeled as strain localizations in a continuum [e.g., *Choi and Gurnis*, 2008; *Cundall*, 1989; *Gerbault et al.*, 1998; *Lavier et al.*, 2000; *Poliakov et al.*, 1994; *Rice*, 1976; *Rudnicki and Rice*, 1975]. Besides the crustal constitutive model, the treatment of fault as having a finite width is another major difference from the elastic models.

[17] We introduce strain-weakening plasticity in order to address the finite strength of the crust and use SNAC (StGermaiN Analysis of Continua), a parallel, Lagrangian, explicit finite difference code for simulating finite deformation of an elasto-visco-plastic solid in 3-D [*Choi et al.*, 2008]. SNAC combines Mohr-Coulomb plasticity with piecewise-linear strain weakening, in which cohesion is defined as a function that is continuous and linear within each of multiple intervals of plastic strain [*Poliakov and Buck*, 1998; *Choi et al.*, 2008; *Lavier et al.*, 2000].

[18] For the crust, both Lamé constants are 30 GPa, the friction angle is 30° (i.e., friction coefficient of ~0.6) and the initial cohesion is 30 MPa. The density of the crust is 2800 kg/m$^3$ and we ignore the fact that fractured fault zones are generally less dense than intact rocks. The 1 km-wide fault zone differs from the rest of the crust in that the initial cohesion is set to be lower: 25 MPa or 3 MPa. The initial cohesion of 25 MPa allows the fault to sustain tensional stresses before it goes through strain weakening and is assigned to the models with a single releasing bend. The lower 3 MPa initial cohesion substantially lowers frictional resistance along the fault and is assigned to the paired bend models. The effects of relatively strong and weak faults are further discussed below. The rate of cohesion decrease as a function of accumulated plastic strain is governed by the strain weakening modulus (Figure 3b). The value used in this study is −167 MPa for both normal crust and fault zone (the negative sign indicates weakening). Strain weakening is activated when the plastic strain becomes 1% and saturates at 10%. With these values, cohesion is reduced by 15 MPa over 9% of plastic strain and the minimum cohesion of the crust and of the more cohesive fault zones are 15 and 10 MPa, respectively. In all cases, cohesion values have a lower bound of 0.1 MPa. The strength of the fault can be also expressed by a friction coefficient, which has been empirically shown to be significantly lowered during dynamic (co-seismic) loading [e.g., *Marone*, 1998; *Niemeijer et al.*, 2010]. The variation of friction coefficient on a tectonic time scale is little constrained although most of the long-term displacement on real upper crustal faults accumulates by coseismic slip events, justifying low friction coefficients. However, addressing how faults are actually weakened is beyond the scope of this study. Later, we discuss model behavior that can be attributed to cohesion reduction, our only way to weaken the fault.

[19] The model domain has the dimensions of 40 × 32 × 20 km and is discretized into 80 × 64 × 40 elements. Although the domain is smaller than in elastic models, the resolution is about 500 m, four times higher. In contrast to the zero-thickness assumption made for the elastic models, the fault is resolved by two elements and therefore is about 1 km wide. The model initially has no topography and is in equilibrium with gravitational load. As in the elastic models, the right-lateral motion of 2 cm/yr is applied on the fault-parallel vertical boundaries and the $z$ component of velocity

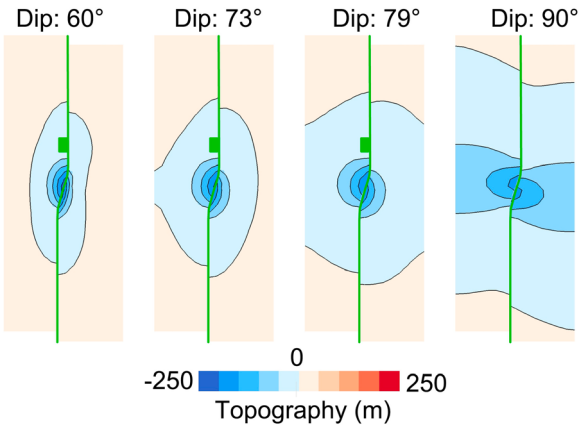


**Figure 4.** Topography of elastic models with a single releasing bend after 3 km of strike-slip motion (map view). Contours of topography (black solid lines) have a 50 m interval. The green line depicts the surface trace of a curtain. Note that the grid has been displaced by the displacement field.

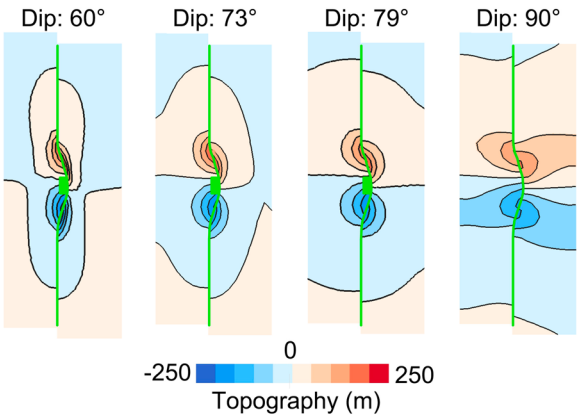


**Figure 5.** Same as Figure 4 but for models with a paired bend.

is zero on the two fault-normal vertical faces (*xz* planes) (Figure 3a). The *xz* planes are additionally supported by lithostatic pressure. The bottom boundary is free to slip horizontally but is fixed in the vertical direction. The top boundary is a free surface. These models were run until the total applied right-lateral motion reached 3 km.

## 3. Results

### 3.1. Elastic Responses

[20] The vertical displacements at the top surface of purely elastic crust cut by a transcurrent fault with a single releasing bend are shown in Figure 4. The subsidence around the bend is attributed to the Poisson's effect caused by the applied fault slip and strike-slip motion. It would be gravitational collapse rather than the Poisson's effect that causes surface depression and a nonzero dip component in fault slip vectors if fault kinematics was not completely constrained as in these simplistic models and gravitational body forces were included. Nonetheless, two trends in the surface deformation with the increasing dip angle are noticeable. First, the subsided area increases as the dip of the curtain increases. Both the size and reach of the force causing subsidence increase as $D$ increases because $W$ is fixed. Increasing the depth of the curtain (larger $D$) increases the volume deficit and its average depth. Thus the negative surface force increases and is more widely distributed. More importantly, the degree of asymmetry in terms of the subsided area is greater for the shallower dipping curtains, i.e., the hanging wall deforms more than the footwall when the curtain has a low dip but the difference progressively vanishes as the dip increases. Although subtle compared to the elasto-plastic models, this trend is consistent with them and with observations.

[21] Elastic models with paired bends display both subsidence at the releasing bend and uplift due to compression at the restraining bend (Figure 5). This correlation of topography with the bend types and the increasing asymmetry with decreasing dip angle are also seen in these models. In addition, the pattern of vertical displacements exhibit mirror symmetry to some degree with respect to the domain-centered conjugate plane to the fault. These two trends persist despite boundary effects that we verify by doing the same calculations in an increased-size domain (Figure 6).

### 3.2. Elasto-Plastic Responses to a Single Releasing Bend

[22] The asymmetry of basins across a releasing bend is greater in inverted-curtain models that include plastic yielding (Figure 7). As in the previous purely elastic models, the asymmetry vanishes for a vertical bend. The magnitude of basin subsidence is greater in the elasto-plastic models and the wavelength of the basins is smaller, as might be expected if the system yields inelastically. In our elastic models faults are "welded" and off-fault stresses and deformation related to the bends are high. In contrast, weak elasto-plastic faults of finite thickness respond to stresses in all directions and they can absorb most of the extension at the releasing bends. This weakness lowers the stress, which may then be too weak to cause yielding on either side of the fault. As a result, little or no footwall block deformation occurs, although gravitational collapse of the hanging wall can still occur due to the loss of support. The concentration of strain in the fault zone is characteristic of the elasto-plastic models but not of the purely elastic models.

[23] Our elasto-plastic models of releasing bends are similar to the corresponding purely elastic models in that the area

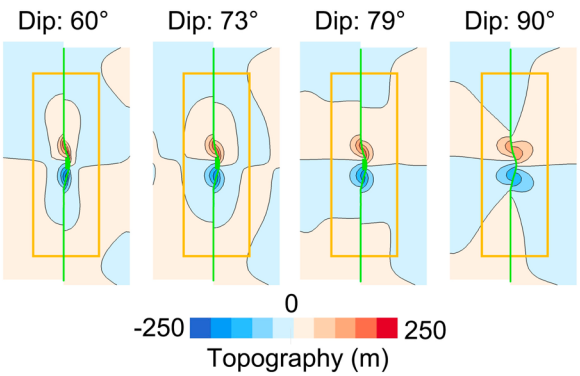


**Figure 6.** Same as Figure 5 but for a larger horizontal dimensions: 100 × 64 km. The area outlined by an orange-colored box corresponds to the original domain size.

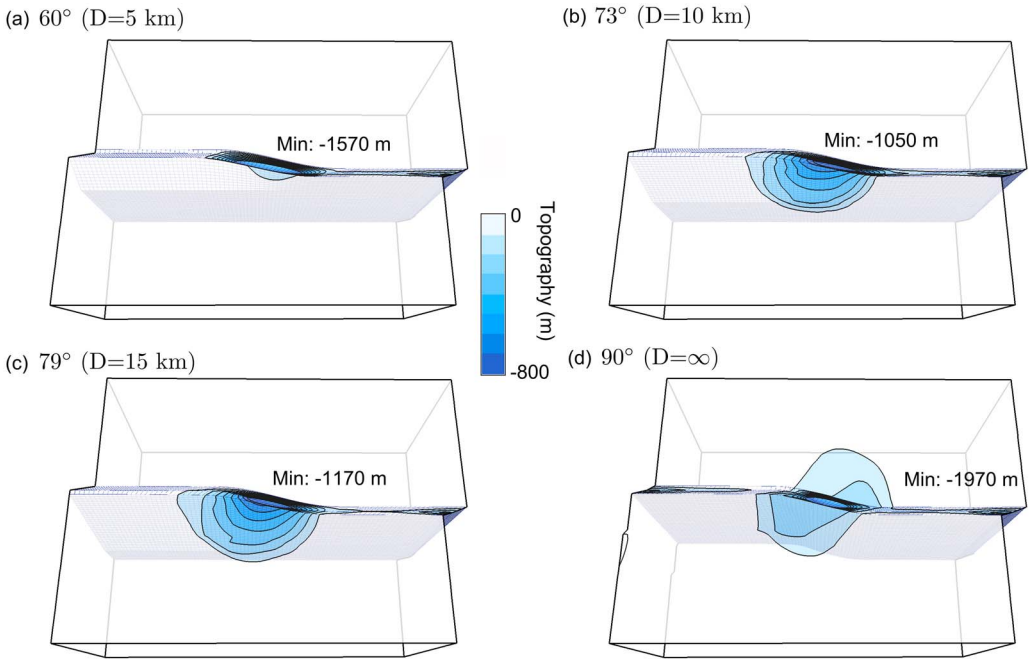


**Figure 7.** Topography, contoured on top of the deformed elasto-plastic model domain after 3 km of slip for a single releasing bend. The corresponding curtains dip at (a) 60°, (b) 73°, (c) 79°, and (d) 90°. The contour internal is 100 m. The deformed configuration of the fault zone is represented by the mesh within the domain. The minimum topography (marked) occurs within the fault zone in all cases.

of off-fault subsidence increases as the dip angle increases from 60° to 79° (Figures 7a–7c). An obvious difference is that the asymmetric basin growth in the elasto-plastic models has been intensified to such a degree that no significant deformation occurs on the footwall side. Plastic behavior intensifies the asymmetry because when the hanging wall side of the fault yields, the stress diminishes on both sides and the footwall side does not yield. In this, the model is realistic not only in what happens, but also in why it happens. When the curtain is vertical the asymmetry vanishes and a relatively small amount of off-fault deformation occurs on both sides of the fault although most of the extension is accommodated by the fault zone itself (Figure 7d).

### 3.3. Elasto-Plastic Responses to a Paired Bend

[24] We first depict the general model behavior as temporal changes in surface topography, plastic strain and velocity fields in Figure 8. The applied boundary motion (Figure 8a) generates distributed shearing within two crustal blocks in the early phase, but deformation starts to concentrate in the near-fault region after about 1 km of slip, when the fault zone yields (Figure 8b). With continued imposed strike-parallel motion, the central fault zone absorbs most of this motion. As a result, the crust on each side of the fault behaves like a rigid block at a distance greater than W (Figure 8c). Surface topography also starts to show the expected uplift and subsidence – a ridge and a basin – associated with the restraining and releasing bends, respectively. As plastic strain continues to increase with applied motion, topographic relief also increases (Figure 8d).

[25] The size and relief of structures created at releasing and restraining bends depends on the depth (or dip angle) of the curtain. As depth increases, relief generally decreases. Ridge heights and basin depths are 670 m and −1800 m for the 60°-dip curtain (Figure 9a), respectively, versus 160 m and −1100 m for the 79° one (Figure 9c). A caveat is that, on the releasing bend of the shallow curtain (dip 60°), subsidence is confined to the

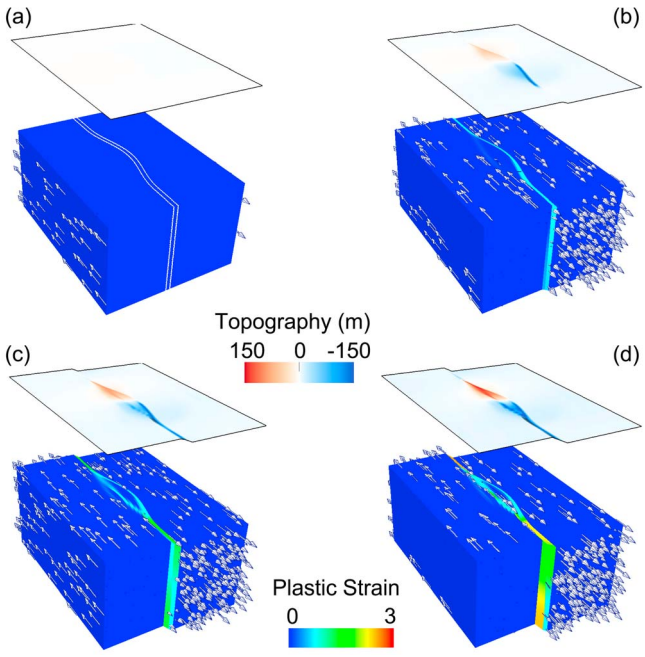


**Figure 8.** Velocity (3D arrows), plastic strain fields and surface topography associated with a paired bend that is formed by the 79°-dipping curtain. After slip of (a) 0 km, (b) 1 km, (c) 2 km, and (d) 3.0 km.

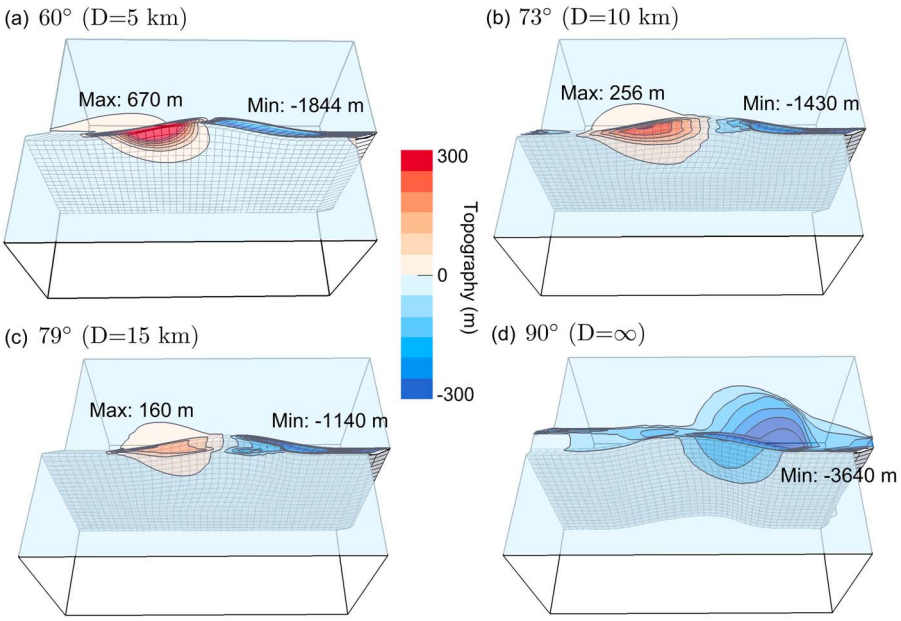


**Figure 9.** Same as Figure 7 but for the paired bend models with a curtain dipping at (a) 60°, (b) 73°, (c) 79° and (d) 90°. The topography contours have a 50 m interval. When saturated in the given color scale, the minimum or maximum of topography is denoted.

fault zone (Figure 9a). The space problem associated with this shallow bend can apparently be accommodated exclusively by deformation within the weak fault zone. The 3-km displacement imposed in the model may not be sufficient to cause off-fault deformation in transtension. It does cause off-fault deformation in transpression, however, and for this shallow curtain the area of uplift is much larger than the area of subsidence. As the relief decreases with increasing dip angle of the curtain, uplift and subsidence tend toward similar areal extents. While in the 60°-dipping model uplift is the dominant mode of deformation in the off-fault area, the area of subsidence becomes roughly equal to that of uplift in the 79°-dipping model. This behavior may also reflect the trade-off between deformation within and outside the fault zone. Finally, the distribution of subsidence changes dramatically in the case of the vertical curtain, where both sides of the fault subsided (Figure 9d). The restraining bend is shunted by a new fault before any uplift occurs. As a result, the overall behavior is similar to that of a single releasing bend by a vertical curtain. However, the vertical case still displays asymmetric relief, with greater subsidence on the convex side of the extensional bend because this side is farther from the restraining bend and thus less affected by it. It is also the footwall side where subsidence is less or absent in finite inverted curtains (Figures 5 and 7) and in real analogs. This discrepancy is thus consistent with the hypothesis that fault bends tend to attenuate with depth.

[26] The most important result of this study is that the relief associated with inverted curtains is generally asymmetric relative to the fault. The relief grows mainly on the hanging wall side of the fault (Figure 9). This asymmetry is more pronounced in the ridges than in the basins. The proximity of a restraining bend appears to reduce the size of the basins formed at the releasing bend. The cases with a single bend show simpler patterns of deformation than those with a paired bend due to the lack of interaction between releasing and restraining bends.

## 4. Discussion and Summary

[27] Our modeling of the kinematic response to releasing bends along strike-slip faults supports the concept that one-sided asymmetric transform basins are associated with "inverted curtain" structures, where the fault is non-vertical and the amplitude of the bend decreases with depth. As observed in real cases, subsidence (uplift) in these releasing (restraining) bends is generally concentrated on the hanging wall side in both elastic and elasto-plastic models. This behavior is more pronounced in elasto-plasic models that can yield, but is also seen in the elastic models. Models show that it is the geometry of the dipping curtains that causes the hanging wall and footwall to respond differently to transform motion. Because kinematics of relative motion at a releasing bend is such that space is newly created between the two crustal blocks, the hanging wall loses support and thus becomes gravitationally unstable. Confirming this simple physics, our elasto-plastic models develop one-sided basins at releasing bends. In these models, basins form only on the hanging wall side of such 3D bends, in line with observations along the North Anatolian Fault and other continental transform faults [*Seeber et al.*, 2010]. All the models with a vertical curtain produce quasi-symmetrical relief about the fault, markedly different from dipping curtains and from geologic examples. Finally, asymmetric basin formation persists through changes in model parameters and seems robust. In summary, we have verified our hypothesis that sub-surface fault geometry can be a sole origin of one-sided basin formation at releasing bends in a crust of finite strength.

[28] In the elasto-plastic models with a steep curtain and a paired bend, the imposed fault geometry was unstable. For

such cases a new fault was created even with the relatively small displacement of the model runs. Bend-related stresses apparently cause yielding outside the prescribed fault zone and the locus of shear shifts away from the original bent fault geometry to a new straighter fault. The critical factor in this behavior is again the curtain's dip. Such shunting occurs only when the curtain has a large dip such as 79° and 90° (Figures 9c and 9d). In the deep (dip 79°) curtain, a new band of strain shunts the imposed symmetrical double bend – the inverted curtain – and connects the original fault system on either side of the curtain, forming a new straight and continuous strike-slip fault. Both ridge and basin are confined between the original warped fault trace and the new straight segment (Figure 9c). Similarly, the vertical paired-bend curtain spawns a new fault that shunts the restraining bend, but retains the releasing bend (Figure 9d). In these cases, the height and width of bend-associated ridges and basins depend on when and how shunting occurs. The new fault was created after about 2 km of strike-slip motion in the 79° curtain model with a low value of initial cohesion. When the cohesion of the fault zone was increased, shunting of the curtain occurred after an even smaller strike-slip motion. By shunting the bends, these new faults allow fault-parallel motion everywhere and thus eliminate relief growth. They are not auxiliary faults that would facilitate it. In general, extensional bends are more likely to persist in our models, which is consistent with recent suggestions that strain partitioning is more common in transpression than in transtension (Seeber et al., submitted manuscript, 2011) and with the high stress suggested by secondary structures at restraining bends [e.g., *Cowgill et al.*, 2004].

[29] Although shunting of fault bends may occur in nature, some fault bends are known to persist through large fault displacements and basins can continue to develop over geologic time. For example, the Ridge Basin in southern California continued to grow for 7 million years reaching a length of 70 km [*Crowell*, 2003]. Available models cannot yet reproduce such "steady-state" growth of transform basins. For a restraining bend to survive a continued transform motion, the magnitude of shear and normal tractions on the fault surface at the restraining bend would have to be kept lower than is possible in current rheological models. Such a weak rheology might be realizable through reduction in friction coefficient, which is justified by numerous lab experiments [e.g., *Marone*, 1998; *Niemeijer et al.*, 2010]. Erosion and sedimentation would also diminish the resistance from topographic stress to the growth of basins and push-ups and may also need to be included in the models. It is likely that instability of the imposed fault geometry seen in some of our models reflects the unrealistic finiteness of the model domain.

[30] A general description of fault-bend stability would require a systematic study of the fault system's sensitivity to many parameters such as the bend geometry, elastic stiffness, yield strength and strain weakening. Such a study is beyond the scope of this investigation. Preliminary attempts found insignificant changes in the results for models with the same set of bend geometries but with lower values of Lamé constants (10 GPa). The difference in initial cohesion, lower within than outside the fault zone, is the only representation of the fault and is clearly important. The system appears to be very sensitive to the width of the fault zone and the initial cohesion ratio. In contrast, no significant changes in model behavior were incurred when the strain weakening modulus was reduced to zero (i.e., plastic parameters were kept constant). The fault zone is itself the site of maximum subsidence in the models because of the lower cohesion within the finite width of this zone and the assumed incompressibility during plastic deformation (Figure 7 and 9). The wider or weaker is the fault zone relative to non-damaged crustal material, the more the component of bend-related deformation normal to the fault tends to be accommodated by the fault zone itself. The greater compliance in the fault zone may correctly represent the resistance to fault-parallel shear, but is likely to over-estimate compliance in other strain components. If cohesion is increased in a paired bend model, the restraining bend is shunted by a new fault after a small amount of fault offset. One of the main challenges for this research effort is a more mechanically realistic model of the fault and boundary conditions.

[31] Much room for improvement is left in terms of long-term evolution of structures such as the migration of bends and the evolution of basins and ridges associated with long-lived bends. Also, larger deformations than those presented in this study will be able to produce more realistic deformation models that can be compared with real basins and ridges associated with continental transform faults where accumulated displacements are typically in the many tens of kilometers.

[32] Greater fault-offset models will eventually provide an opportunity to constrain the strain-weakening parameters through comparison with the tilt rate of originally horizontal turbidite layers that are observed in many transform basins such as the one in the Gulf of Izmit. What still remains to be improved with regard to our knowledge of fault weakening includes the level of cohesion for intact crust and fault zone as well as the appropriate amount and rate of cohesion reduction as a function of fault offset. As we discussed earlier, a very low friction angle might be necessary for a long-surviving restraining bend. Geologically constrained models for long-term evolution of transform bends will allow the exploration of other effects, including friction coefficient.

[33] **Acknowledgments.** We thank an anonymous reviewer for constructive comments and Marcel Frehner for a very helpful and detailed review. This work was supported by U.S. National Science Foundation grant EAR 09-11565 and OCE 09-28447 and in part through TeraGrid resources provided by Texas Advanced Computing Center under grant TG-EAR100019.

## References

Aagaard, B., C. Williams, and M. Knepley (2007), PyLith: A finite-element code for modeling quasi-static and dynamic crustal deformation, *Eos Trans. AGU*, *88*(52), Fall Meet. Suppl., Abstract T21B-0592.

Aagaard, B., C. Williams, M. Knepley (2008), PyLith: A finite-element code for modeling quasi-static and dynamic crustal deformation, *Eos Trans. AGU*, *89*(53), Fall Meet. Suppl., Abstract T41A-1925.

Armijo, R., B. Meyer, G. C. P. King, A. Rigo, and D. Papanastassiou (1996), Quaternary evolution of the Corinth Rift and its implication for the Late Cenozoic evolution of the Aegean, *Geophys. J. Int.*, *126*, 11–53, doi:10.1111/j.1365-246X.1996.tb05264.x.

Armijo, R., B. Meyer, A. Hubert, and A. Barka (1999), Westward propagation of the north Anatolian fault into the northern Aegean: Timing the kinematics, *Geology*, *27*(3), 267–270, doi:10.1130/0091-7613(1999)027<0267:WPOTNA>2.3.CO;2.

Bécel, A., M. Laigle, B. de Voogd, A. Hirn, T. Taymaz, S. Yolsal-Cevikbilen, and H. Shimamura (2010), North Marmara Trough architecture of basin infill, basement and faults, from PSDM reflection and OBS refraction seismics, *Tectonophysics*, *490*, 1–14, doi:10.1016/j.tecto.2010.04.004.

Ben-Avraham, Z., V. Lyakhovsky, and G. Schubert (2010), Drop-down formation of deep basins along the Dead Sea and other strike-slip fault systems, *Geophys. J. Int.*, *181*, 185–197, doi:10.1111/j.1365-246X.2010.04525.x.

Brace, W. F., and D. L. Kohlstedt (1980), Limits on lithospheric stress imposed by laboratory experiments, *J. Geophys. Res.*, *85*(B11), 6248–6252, doi:10.1029/JB085iB11p06248.

Buiter, S. J. H., R. S. Huismans, and C. Beaumon (2008), Dissipation analysis as a guide to mode selection during crustal extension and implications for the styles of sedimentary basins, *J. Geophys. Res.*, *113*, B06406, doi:10.1029/2007JB005272.

Byerlee, J. (1978), Friction of rocks, *Pure Appl. Geophys.*, *116*, 615–626, doi:10.1007/BF00876528.

Calais, E., A. Freed, G. Mattioli, F. Amelung, S. Jonsson, P. Jansma, S.-H. Hon, T. Dixon, C. Prépetit, and R. Momplaisir (2010), Transpressional rupture of an unmapped fault during the 2010 Haiti earthquake, *Nat. Geosci.*, *3*, 794–799, doi:10.1038/ngeo992.

Carton, H., et al. (2009), Seismic evidence for Neogene and active shortening offshore of Lebanon (Shalimar cruise), *J. Geophys. Res.*, *114*, B07407, doi:10.1029/2007JB005391.

Choi, E., and M. Gurnis (2008), Thermally induced brittle deformation in oceanic lithosphere and the spacing of fracture zones, *Earth Planet. Sci. Lett.*, *269*, 259–270, doi:10.1016/j.epsl.2008.02.025.

Choi, E., L. Lavier, and M. Gurnis (2008), Thermomechanics of midocean ridge segmentation, *Phys. Earth Planet. Inter.*, *171*, 374–386, doi:10.1016/j.pepi.2008.08.010.

Collettini, C., A. Niemeijer, C. Viti, and C. Marone (2009), Fault zone fabric and fault weakness, *Nature*, *462*, 907–910, doi:10.1038/nature08585.

Coney, P. J. (1980), Cordilleran metamorphic core complexes, in *Cordilleran Metamorphic Core Complexes*, edited by M. D. Crittenden, P. J. Coney, and G. H. Davis, *Mem. Geol. Soc. Am.*, *153*, 7–34.

Cormier, M. -H., et al. (2006), The North Anatolian fault in the Gulf of Izmit (Turkey): Rapid vertical motion in response to minor bends of a non-vertical continental transform, *J. Geophys. Res.*, *111*, B04102, doi:10.1029/2005JB003633.

Cowgill, E., J. R. Arrowsmith, A. Yin, X. Wang, and Z. Chen (2004), The Akato Tagh bend along the Altyn Tagh Fault, northwest Tibet 2: Active deformation and the importance of transpression and strain hardening within the Altyn Tagh system, *Geol. Soc. Am. Bull.*, *116*(11), 1443–1464, doi:10.1130/B25360.1.

Crowell, J. C. (2003), Tectonics of Ridge Basin region, Southern California, in *Evolution of Ridge Basin, Southern California; An Interplay of Sedimentation and Tectonics*, edited by J. C. Crowell, *Spec. Pap. Geol. Soc. Am.*, *367*, 157–203.

Cundall, P. (1989), Numerical experiments on localization in frictional materials, *Ing. Arch.*, *59*, 148–159, doi:10.1007/BF00538368.

Davis, G., and G. Lister (1988), Detachment faulting in continental extension: Perspectives from the southwestern U.S. Cordillera, in *Processes in Continental Lithospheric Deformation*, edited by S. P. J. Clark et al., *Spec. Pap. Geol. Soc. Am.*, *218*, 133–159.

Dibblee, T. W., Jr. (1977), Strike-slip tectonics of the San Andreas Fault and its role in Cenozoic basin evolvement, in *Late Mesozoic and Cenozoic Sedimentation and Tectonics in California*, edited by T. H. Nilsen, pp. 26–38, San Joaquin Geol. Soc., Bakersfield, Calif. [Reprinted in *Wrench Fault Tectonics*, *AAPG Reprint Ser.*, vol. 28, edited by A. G. Sylvester, pp. 159–172, Am. Assoc. of Pet. Geol., Tulsa, Okla., 1984.]

Eusden, J. D., J. R. Pettinga, and J. K. Campbell (2000), Structural evolution and landscape development of a collapsed transpressive duplex on the Hope Fault, North Canterbury, New Zealand, *N. Z. J. Geol. Geophys.*, *43*(3), 391–404, doi:10.1080/00288306.2000.9514896.

Gerbault, F., A. N. B. Poliakov, and M. Daignieres (1998), Prediction of faulting from the theories of elasticity and plasticity: What are the limits?, *J. Struct. Geol.*, *20*, 301–320, doi:10.1016/S0191-8141(97)00089-8.

Hayes, G. P., et al. (2010), Complex rupture during the 12 January 2010 Haiti earthquake, *Nat. Geosci.*, *3*, 800–805, doi:10.1038/ngeo977.

Hergert, T., and O. Heidbach (2010), Slip-rate variability and distributed deformation in the Marmara Sea fault system, *Nat. Geosci.*, *3*, 132–135, doi:10.1038/ngeo739.

Hornbach, M. J., et al. (2010), High tsunami frequency as a result of combined strike-slip faulting and coastal landslides, *Nat. Geosci.*, *3*, 783–788, doi:10.1038/ngeo975.

Katzman, R., U. S. ten Brink, and J. Lin (1995), Three-dimensional modeling of pull-apart basins; implications for the tectonics of the Dead Sea Basin, *J. Geophys. Res.*, *100*(B4), 6295–6312, doi:10.1029/94JB03101.

Lachenbruch, A. H., and J. H. Sass (1992), Heat Flow From Cajon Pass, fault strength, and tectonic implications, *J. Geophys. Res.*, *97*(B4), 4995–5015, doi:10.1029/91JB01506.

Lavier, L. L., W. R. Buck, and A. N. B. Poliakov (2000), Factors controlling normal fault set in an ideal brittle layer, *J. Geophys. Res.*, *105*(B10), 23,431–23,442, doi:10.1029/2000JB900108.

Le Pichon, X., et al. (2001), The active Main Marmara Fault, *Earth Planet. Sci. Lett.*, *192*, 595–616, doi:10.1016/S0012-821X(01)00449-6.

Li, Q., M. Liu, and H. Zhang (2009), A 3-D viscoelastoplastic model for simulating long-term slip on non-planar faults, *Geophys. J. Int.*, *176*, 293–306, doi:10.1111/j.1365-246X.2008.03962.x.

Mann, P. (2007), Global catalogue, classification and tectonic origins of restraining- and releasing bends on active and ancient strike-slip fault systems, in *Tectonics of Strike-Slip Restraining and Releasing Bends*, edited by W. D. Cunningham and P. Mann, *Geol. Soc. Spec. Publ.*, *290*, 13–142.

Marone, C. (1998), Laboratory-derived friction laws and their application to seismic faulting, *Annu. Rev. Earth Planet. Sci.*, *26*(1), 643–696, doi:10.1146/annurev.earth.26.1.643.

McAdoo, D., J. Caldwell, and D. Turcotte (1978), On the elastic-perfectly plastic bending of the lithosphere under generalized loading with application to the Kurd Trench, *Geophys. J. R. Astron. Soc.*, *54*(1), 11–26.

McGarr, A., and N. C. Gay (1978), State of Stress in the Earth's Crust, *Annu. Rev. Earth Planet. Sci.*, *6*(1), 405–436, doi:10.1146/annurev.ea.06.050178.002201.

Mount, V. S., and J. Suppe (1987), State of stress near the San Andreas fault: Implications for wrench tectonics, *Geology*, *15*(12), 1143–1146, doi:10.1130/0091-7613(1987)15<1143:SOSNTS>2.0.CO;2.

Nicholson, C., and L. Seeber (1989), Evidence for contemporary block rotation in strike-slip environments: Examples from the San Andreas fault system, southern California, in *Paleomagnetic Rotations and Continental Deformation*, edited by C. Kissel and C. Laj, pp. 247–280, Kluwer Acad., Dorcrecht, Netherlands.

Niemeijer, A., C. Marone, and D. Elsworth (2010), Fabric induced weakness of tectonic faults, *Geophys. Res. Lett.*, *37*, L03304, doi:10.1029/2009GL041689.

Okay, A., and N. Okay (2002), Tectonically induced Quaternary drainage diversion in the northeastern Aegean, *J. Geol. Soc.*, *159*(4), 393–399, doi:10.1144/0016-764901-065.

Okay, A., E. Demirbag, H. Kurt, N. Okay, and I. Kuscu (1999), An active, deep marine strike-slip basin along the North Anatolian Fault in Turkey, *Tectonics*, *18*(1), 129–147, doi:10.1029/1998TC900017.

Okay, A., A. Kaşhlar-Özcan, C. Imren, A. Boztepe-Güney, E. Demirbag, and I. Kuşçu (2000), Active faults and evolving strike-slip basins in the Marmara Sea, Northwest Turkey: A multi-channel seismic reflection study, *Tectonophysics*, *321*, 189–218, doi:10.1016/S0040-1951(00)00046-9.

Okay, A., O. Tuysuz, and S. Kaya (2004), From transpression to transtension: Changes in morphology and structure around a bend on the North Anatolian Fault in the Marmara region, *Tectonophysics*, *391*, 259–282, doi:10.1016/j.tecto.2004.07.016.

Pantosti, D., S. Pucci, N. Palyvos, P. M. D. Martini, G. D'Addezio, P. E. F. Collins, and C. Zabci (2008), Paleoearthquakes of the duzce fault (north anatolian fault zone); insights for large surface faulting earthquake recurrence, *J. Geophys. Res.*, *113*, B01309, doi:10.1029/2006JB004679.

Poliakov, A., and W. Buck (1998), Mechanics of stretching elastic-plastic-viscous layers:Applications to slow-spreading mid-ocean ridges, in *Faulting and Magmatism at Mid-Ocean Ridges*, *Geophys. Monogr. Ser.*, vol. 106, edited by W. R. Buck et al., pp. 305–324, AGU, Washington, D. C.

Poliakov, A., H. Hermann, Y. Podladchikov, and S. Roux (1994), Fractal plastic shear bands, *Fractals*, *2*, 567–581, doi:10.1142/S0218348X9400079X.

Prentice, C., P. Mann, T. Crone, R. Gold, K. Hudnut, R. Briggs, R. Koehler, and P. Jean (2010), Seismic hazard of the Enriquillo-Plantain Garden fault in Haiti inferred from paleoseismology, *Nat. Geosci.*, *3*, 789–793, doi:10.1038/ngeo991.

Rice, J. R. (1976), The localization of plastic deformation, in *Proceedings of the 14th International Congress on Theoretical and Applied Mechanics*, edited by W. T. Koiter, pp. 207–220, North-Holland, New York.

Rudnicki, J., and J. Rice (1975), Conditions for the localization of deformation in pressure-sensitive dilatant materials, *J. Mech. Phys. Solids*, *23*, 371–394, doi:10.1016/0022-5096(75)90001-0.

Seeber, L., O. Emre, M. -H. Cormier, C. C. Sorlien, C. M. G. McHugh, A. Polonia, N. Ozer, and N. Catagay (2004), Uplift and subsidence from oblique slip: The Ganos-Marmara bend of the North Anatolian Transform, Western Turkey, *Tectonophysics*, *391*, 239–258, doi:10.1016/j.tecto.2004.07.015.

Seeber, L., M. H. Cornier, C. McHugh, O. Emre, A. Polonia, and C. Sorlien (2006), Rapid subsidence and sedimentation from oblique slip near a bend on the North Anatolian Transform in the Marmara Sea, Turkey, *Geology*, *34*(11), 933–936, doi:10.1130/G22520A.1.

Seeber, L., C. Sorlien, M. Steckler, and M. -H. Cormier (2010), Continental transform basins: Why are they asymmetric?, *Eos Trans. AGU*, *91*(4), 29, doi:10.1029/2010EO040001.

Segall, P., and D. D. Pollard (1980), Mechanics of discontinuous faults, *J. Geophys. Res.*, *85*(B8), 4337–4350, doi:10.1029/JB085iB08p04337.

Townend, J., and M. D. Zoback (2000), How faulting keeps the crust strong, *Geology*, *28*(5), 399–402, doi:10.1130/0091-7613(2000)28<399:HFKTCS>2.0.CO;2.

Wakabayashi, J. (2007), Stepovers that migrate with respect to affected deposits: Field characteristics and speculation on some details of their evolution, in *Tectonics of Strike-Slip Restraining and Releasing Bends*, edited by W. D. Cunningham and P. Mann, *Geol. Soc. Spec. Publ.*, *290*, 169–188.

Wernicke, B. (1981), Low-angle normal faults in the Basin and Range Province: Nappe tectonics in an extending orogen, *Nature*, *291*, 645–648, doi:10.1038/291645a0.

Williams, C. A. (2006), Development of a package for modeling stress in the lithosphere, *Eos Trans. AGU*, *87*(36), Jt. Assem. Suppl., Abstract T24A-01.

Williams, C. A., B. Aagaard, and M. G. Knepley (2005), Development of software for studying earthquakes across multiple spatial and temporal scales by coupling quasi-static and dynamic simulations, *Eos Trans. AGU*, *86*(52), Fall Meet. Suppl., Abstract S53A-1072.

Wu, J. E., K. McClay, P. Whitehouse, and T. Dooley (2009), 4D analogue modeling of transtensional pull-apart basins, *Mar. Pet. Geol.*, *26*(8), 1608–1623, doi:10.1016/j.marpetgeo.2008.06.007.

Zoback, M. D., and J. H. Healy (1992), In situ stress measurements to 3.5 km depth in the Cajon Pass Scientific Research Borehole: Implications for the mechanics of crustal faulting, *J. Geophys. Res.*, *97*(B4), 5039–5057, doi:10.1029/91JB02175.

R. Buck, E. Choi, L. Seeber, and M. S. Steckler, Lamont-Doherty Earth Observatory, P.O. Box 1000, 61 Rt. 9W, Palisades, NY 10964, USA. (echoi@ldeo.columbia.edu)